The Discrete Orthogonal Polynomial Least Squares Method for Approximation and Solving Partial Differential Equations

Anne Gelb*, Rodrigo B. Platte and W. Steven Rosenthal

Department of Mathematics and Statistics, Arizona State University, Tempe, Arizona 85287, USA.

Abstract. We investigate numerical approximations based on polynomials that are orthogonal with respect to a weighted discrete inner product and develop an algorithm for solving time dependent differential equations. We focus on the family of super Gaussian weight functions and derive a criterion for the choice of parameters that provides good accuracy and stability for the time evolution of partial differential equations. Our results show that this approach circumvents the problems related to the Runge phenomenon on equally spaced nodes and provides high accuracy in space. For time stability, small corrections near the ends of the interval are computed using local polynomial interpolation. Several numerical experiments illustrate the performance of the method.

1 Introduction

This paper investigates a high order numerical method for approximating smooth functions on a uniform grid and solving partial differential equations on a hybrid grid in $[-1,1]$. The method uses the discrete orthogonal polynomial least squares (DOP-LS) approximation based on the *super Gaussian weight function*, which is both smoothly connected to zero at ± 1 and equals one in nearly the entire domain. As a result, the method has fast decaying expansion coefficients and also successfully suppresses Runge oscillations that pollute the boundary regions. Such desirable weight function features were

---

*Corresponding author. *Email addresses:* `ag@math.la.asu.edu` (A. Gelb), `platte@math.la.asu.edu` (R. B. Platte), `William.Rosenthal@asu.edu` (W. S. Rosenthal)

first exploited in [17] in the context of spectral reprojection from (pseudo-)spectral Fourier data, and later in [15] as a least squares approximation technique for piecewise smooth functions given equally or arbitrarily spaced points. In [17], the Fourier coefficients were reprojected onto the Freud polynomial basis (what we will refer to as a super Gaussian polynomial basis) to eliminate the Gibbs phenomenon. The concept of reprojection from the Fourier basis onto another basis to remove the Gibbs phenomenon has been discussed at length in the context of Gegenbauer reconstruction, see [20, 21] and references therein. The Gibbs phenomenon is removed due to the reprojection polynomial weight function being smoothly connected to zero near the boundaries, which prevents the Gibbs oscillations in the Fourier approximation from entering the reprojection and allows rapid decay of the reprojection expansion coefficients. However, the Gegenbauer polynomials are not entirely satisfactory as a reprojection basis due to their high propensity to round-off error. Furthermore, for large orders, the Gegenbauer partial sum expansion behaves like a power series, yielding what was coined the generalized Runge phenomenon in [2]. In contrast, as mentioned above, the super Gaussian weight functions are designed to be one in nearly the entire domain of approximation, so that the growth of the corresponding polynomials is better controlled. The approximation also utilizes more information from the underlying function. In [15] it was noted that the values given on equidistant grid points need not first be converted to pseudo-spectral Fourier coefficients in order to recover a highly accurate approximation. The resulting super Gaussian *discrete orthogonal polynomial least squares* (DOP-LS) method was shown to be robust and efficient for the approximation of smooth functions.

This investigation further analyzes the super Gaussian DOP-LS approximation of smooth functions in $[-1,1]$ when the function is known at uniform grid points. We extend the analysis from [15] to characterize the optimal parameters needed for convergence in $[-1,1]$, as well as in smaller intervals $[-\delta,\delta]$, $0 < \delta < 1$. This information is then used to develop a new hybrid multi-domain method for the approximation of smooth functions. The technique consists of "patching" the super Gaussian approximation in $[-\delta,\delta]$ with Chebyshev (interpolatory) approximations in the two smaller boundary regions $[-1,-\delta]$ and $[\delta,1]$ on Gauss Lobatto grids. The combined method enables high order approximation of smooth functions with less point clustering than the typical orthogonal polynomial approximation methods.

In the second part of this paper we incorporate the hybrid multi-domain approximation into a numerical method that computes partial differential equations with smooth solutions. Fourier pseudo-spectral methods are well suited for solving periodic smooth problems on discrete data. Orthogonal polynomials, such as Chebyshev or Legendre polynomials, are used as basis polynomials for spectral methods solving smooth non-periodic problems. In this case, the grid points must be distributed so that the quadrature used (typically Gauss or Gauss-Lobatto) to calculate the expansion coefficients yields high enough accuracy. Such distributions are always clustered at the ends of the intervals. This is a traditional bottleneck when solving partial differential equations with spectral methods, since explicit time stepping methods require very small time steps on the order

of the smallest spatial scaling in the domain to maintain stability. In their seminal paper, [25], Kosloff and Tal-Ezer introduced the mapped Chebyshev method, which essentially stretches the grid points to resemble a more uniform distribution. Consequently, the severe time stepping restriction can be somewhat relaxed. Other non-classical orthogonal polynomials have been introduced for solving advection diffusion problems, Schröedinger equations, and Poisson equations, e.g. [5,6,12,31], as well as for the reconstruction of piecewise smooth functions, [32]. In all of these studies the quadrature points were either obtained numerically or known explicitly for the integration and subsequent approximation. Here we use a multi-domain approach which does not require a particular grid point distribution for the majority of the domain. The domain is split into three overlapping parts, with the dominant part consisting of equally spaced grid points on the entire interval $[-1,1]$.[†] The super Gaussian DOP-LS approximation yields high accuracy in $[-\delta,\delta]$, but the Runge phenomenon impacts the solution in the small boundary regions $[-1,-\delta]$ and $[\delta,1]$. Hence we correct the approximation in those regions using Chebyshev interpolation on Gauss Lobatto points. The time step restriction is based on the number of points in each Chebyshev domain, which decreases as $\delta \to 1$. By carefully patching the solution across the interior boundaries, we achieve high order accuracy and numerical stability.

Our discussion begins by defining the super Gaussian DOP-LS approximation method for smooth functions on equidistant grid point values in Section 2. Parallels are drawn to the spectral reprojection method. We describe the parameters of the method and how they can be optimized, keeping in mind accuracy and robustness while trying to minimize resolution requirements. In Section 3 we describe our hybrid multi-domain method for solving partial differential equations and discuss its convergence properties. Numerical examples are provided in Section 4. Section 5 summarizes the characteristic features of the super Gaussian DOP-LS approximation method and discusses possible future applications.

2   Discrete orthogonal polynomials and least squares approximations

Let $f(x)$ be a smooth function in $[-1,1]$. Suppose we are given the values of $f(x)$ at some distribution of points, x_j, $j=0,\cdots,N$, and we wish to approximate $f(x)$. The naive approach is to use the Lagrange interpolating polynomial, given by

$$p_N(x) = \sum_{j=0}^{N} f(x_j) L_j(x),$$

where

$$L_j(x) = \prod_{j=0, j \neq k}^{N} \frac{x - x_j}{x_k - x_j}$$

[†]We consider uniform points to relax the time step restriction. Any point distribution can be used, however.

are the *Nth* order Lagrange interpolating polynomials. The approximation error is

$$f(x) = p_N(x) + \frac{f^{(N+1)}(x)}{(N+1)!}(x-x_0)(x-x_1)\cdots(x-x_N).$$

It is well known that when x_j, $j=0,\cdots,N$, are equally spaced, the Lagrange polynomial interpolation does not converge pointwise, and furthermore produces wild oscillations near the boundaries. A better interpolation can be obtained using the Chebyshev point distribution, [7]. Furthermore, for $f(x)$ smooth in $[-1,1]$, the resulting Lagrangian interpolation yields spectral accuracy. A more extended study on interpolation errors for general point distributions is in [10].

There have been many investigations of high order reconstruction methods for (piecewise) smooth functions from uniform grid point data, [8,9,14,15,17,20,21,23,32]. Often the data is first converted into pseudo-spectral Fourier coefficients, as is the case for the (pseudo-)spectral reprojection method, [17,20,21]. The general idea is to reproject the Fourier coefficients onto a new orthogonal polynomial basis that does not require periodicity in the underlying function for its convergence. In [15], the approximating polynomial basis is constructed to be orthogonal in the *discrete sense*, and uses the discrete values $f(x_j)$, $j=0,\cdots,N$, directly. Thus the Fourier pseudo-spectral coefficients are never computed, and there is no reprojection involved. In fact, the method is nothing more than a least squares approximation using discrete orthogonal polynomials, see, e.g., [13,29]. We will use that approach here.

To establish notation and put the discrete orthogonal polynomial least squares (DOP-LS) method into context, we first review both the traditional continuous orthogonal polynomial expansion method in Section 2.1, as well as the Fourier pseudo-spectral reprojection method in Section 2.2.

2.1 Orthogonal polynomial expansion

Recall the orthogonal polynomial series expansion for a smooth function $f(x)$ on $[-1,1]$,

$$\hat{P}_N f(x) = \sum_{k=0}^{N} \hat{a}_k \psi_k^{\omega}(x), \tag{2.1}$$

where $\psi_k^{\omega}(x)$, $k=0,\cdots,N$, are orthogonal polynomials with respect to a weight function $\omega(x) \geq 0$ satisfying

$$(\psi_k^{\omega}, \psi_l^{\omega}) = \hat{h}_k \delta_{kl}. \tag{2.2}$$

Here

$$\hat{h}_k = (\psi_k^{\omega}, \psi_k^{\omega}), \tag{2.3}$$

and the weighted inner product is defined as

$$(u,v) := \int_{-1}^{1} u(x)v(x)\omega(x)dx. \tag{2.4}$$

Due to the orthogonality of $\psi_k^\omega(x)$, the coefficients $\hat{a}_k$ can be obtained by

$$\hat{a}_k = \frac{1}{\hat{h}_k}(f, \psi_k^\omega). \tag{2.5}$$

The exponential decay of $\hat{a}_k$, $k = 0, \cdots, N$, ensures that (2.1) converges exponentially for smooth $f(x)$, [11].

Numerical quadrature is typically needed to evaluate (2.5). Assume that $f(x)$ is known on some distribution of points x_j, $j = 0, \cdots, N$, and that the corresponding quadrature weights $\tilde{\omega}_j$ are determined accordingly. Then the continuous coefficients can be approximated by

$$\tilde{a}_k = \frac{1}{\tilde{h}_k} \sum_{j=0}^{N} f(x_j) \psi_k^\omega(x_j) \tilde{\omega}_j, \tag{2.6}$$

where the normalization constants $\tilde{h}_k$ approximate (2.3) as

$$\tilde{h}_k = \sum_{j=0}^{N} (\psi_k^\omega(x_j))^2 \tilde{\omega}_j. \tag{2.7}$$

If the points x_j, $j = 0, \cdots, N$, have a Gaussian type distribution corresponding to $\psi_k^\omega(x)$, and if the discrete weights $\tilde{\omega}_j$ are accurately evaluated from the points x_j, then $\tilde{a}_k \to \hat{a}_k$ exponentially as $N \to \infty$. Consequently, the pseudo-spectral approximation,

$$I_N f(x) = \sum_{k=0}^{N} \tilde{a}_k \psi_k^\omega(x), \tag{2.8}$$

converges exponentially to smooth $f(x)$ in $[-1, 1]$, [3, 4, 10, 11, 18, 19]. Note that $I_N f$ can be written as an interpolating polynomial approximation

$$I_N f(x) = \sum_{j=0}^{N} f(x_j) g_j(x), \tag{2.9}$$

where

$$g_j(x) = \tilde{\omega}_j \sum_{k=0}^{N} \frac{\psi_k^\omega(x) \psi_k^\omega(x_j)}{\tilde{h}_k},$$

are the cardinal basis functions.

Unfortunately, in applications involving imaging, the point distribution can not be arbitrarily chosen, and is typically not Gaussian, so conventional orthogonal polynomial bases are incompatible. Runge effects ruin the convergence of (2.8), or equivalently (2.9). Moreover, on uniform points, Fourier pseudo-spectral methods yield the Gibbs phenomenon for non-periodic functions.

In the case where the nodal distribution is not arbitrary, it is possible to construct the weight function $\omega(x)$ and corresponding $N+1$ discrete weights $\tilde{\omega}_j$ to regain exponential decay of the expansion coefficients (2.5) for $k=0,\cdots,M$, for some $M<N$. The approximation (2.1) can then be reformulated as a *least squares* orthogonal polynomial method with expansion order M. A suitable weight function in (2.1) and appropriate expansion order, M, underly the construction of the general (pseudo-)spectral reprojection method, [20–22], although this is not how the method is traditionally motivated. Below we review the Fourier pseudo-spectral method to gain insight into how to choose an appropriate weight function and expansion order M for the (discrete) orthogonal polynomial least squares method.

2.2 Fourier pseudo-spectral reprojection

Let us assume that $f(x)$ is a smooth but non-periodic function on $[-1,1]$, known on uniform grid points x_j, $j=0,\cdots,N$, with $x_j=-1+j\Delta x$ and $\Delta x=\frac{2}{N}$. The Fourier pseudo-spectral coefficients are computed as

$$\tilde{f}_k=\sum_{j=0}^{N-1}f(x_j)e^{-ik\pi x_j},$$

for $k=-\frac{N}{2},\cdots,\frac{N}{2}-1$, providing the pseudo-spectral Fourier approximation,

$$I_N^{four}f(x)=\sum_{k=-\frac{N}{2}}^{\frac{N}{2}-1}\tilde{f}_k e^{ik\pi x}. \tag{2.10}$$

To alleviate the Gibbs phenomenon, (2.10) is reprojected onto a new basis, $\psi_k^{\omega}(x)$, defined in (2.2), for $k=0,\cdots,M$, and $M<N$. The $C^q[-1,1]$ weight function $\omega(x)$ of the new basis smoothly transitions to zero at the endpoints by satisfying

$$\left.\frac{d^p\omega}{dx^p}\right|_{x=\pm 1}=0, \tag{2.11}$$

for $p=0,1,2,\cdots,q(N)$, where $q(N)$ correlates to the degree of smoothness of the underlying function $f(x)$. The Fourier pseudo-spectral reprojection method computes the partial sum

$$G_{M,N}f(x)=\sum_{k=0}^{M}\hat{g}_{k,N}\psi_k^{\omega}(x), \tag{2.12}$$

where the coefficients $\hat{g}_{k,N}$ are defined as

$$\hat{g}_{k,N}=\frac{1}{\hat{h}_k}\int_{-1}^{1}I_N^{four}f(x)\psi_k^{\omega}(x)\omega(x)dx. \tag{2.13}$$

Numerical quadrature can be used to evaluate (2.13). Since $I_N^{four} f(x_j) = f(x_j)$ and $\omega(x)$ satisfies (2.11), it is convenient to define the quadrature weights as

$$\tilde{\omega}_j = \begin{cases} \omega(x_j)\frac{\Delta x}{2}, & \text{if } j=0 \text{ or } j=N, \\ \omega(x_j)\Delta x, & \text{otherwise.} \end{cases} \tag{2.14}$$

Hence, since $\omega(x_0) = \omega(x_N) = 0$, the trapezoidal rule yields

$$\tilde{g}_{k,N} = \frac{\Delta x}{\tilde{h}_k} \sum_{j=1}^{N-1} f(x_j)\psi_k^\omega(x_j)\omega(x_j), \tag{2.15}$$

where $\tilde{h}_k$ is defined in (2.7). Note that for $q(N)$ large enough, (2.15) is an exponentially accurate approximation of (2.13), [3]. Furthermore, (2.12) can be rewritten as

$$G_{M,N}f(x) = \sum_{j=1}^{N-1} f(x_j)g_{j,M}(x), \tag{2.16}$$

where

$$g_{j,M}(x) = \omega(x_j)\Delta x \sum_{k=0}^{M} \frac{\psi_k^\omega(x_j)\psi_k^\omega(x)}{\tilde{h}_k}.$$

Remark 2.1.

1. $M = \beta N$ for certain prescribed values of $\beta < 1$ yields exponential convergence of (2.12) or (2.16), assuming that the reprojection polynomials, $\psi_k^\omega(x)$, are chosen to be *Gibbs complementary*, [21]. Specifically, (2.11) must hold for $p = 0, \cdots, q(N)$, and (2.1) must produce (theoretical) exponential convergence to smooth $f(x)$. When $M \to N$, the Gibbs oscillations from the Fourier approximation are re-introduced in the approximation.

2. The Gegenbauer polynomials have weight function $\omega_{geg}(x) = (1-x^2)^{q(N)-\frac{1}{2}}$, which satisfies (2.11). They are therefore Gibbs complementary since their orthogonal polynomial expansion (2.1) converges to $f(x)$ exponentially. In addition, as classical orthogonal polynomials, the three term recurrence relationship for the Gegenbauer polynomials is known explicitly and does not require the calculation of any inner products. It is also possible to determine (2.13) explicitly in terms of the pseudo-spectral Fourier coefficients, making the overall computational cost less expensive than if quadrature is used, [22]. However, as $q(N)$ increases, the region that the weight function is significantly different from zero shrinks to a small interval around $x=0$ in $[-1,1]$. The polynomials grow rapidly in the boundary regions, affecting the approximation both in terms of the Runge phenomenon and round-off error, [2, 16, 17].

3. Gaussian quadrature can be used to compute (2.13). In this case (2.16) is not valid. Moreover, (2.12) is more expensive to compute.

4. As observed in [15], (2.16) allows us to interpret the Fourier pseudo-spectral re-projection method as a least squares approximation based on given (uniform) discrete data $f(x_j)$. Hence the convergence analysis of the pseudo-spectral reprojection method provides insight on how to best determine a suitable polynomial basis for the least squares approximation.

5. For non-classical weight functions that satisfy (2.11), it might be difficult to accurately compute the corresponding continuous orthogonal polynomials, [13]. Hence it was proposed in [15] that it would be more accurate and efficient to use polynomials that are orthogonal in the *discrete* sense. This is examined in the next section.

2.3 Weighted discrete orthogonal polynomials

The discrete orthogonal polynomials are defined using the *discrete* inner product on $[-1,1]$ such that

$$<\phi_k^\omega,\phi_l^\omega>=h_k\delta_{kl}, \tag{2.17}$$

where

$$h_k=||\phi_k^\omega||=<\phi_k^\omega,\phi_k^\omega>. \tag{2.18}$$

Here the weighted discrete inner product is defined by

$$<u,v>:=\sum_{j=0}^{N}u(x_j)v(x_j)\tilde{\omega}_j \tag{2.19}$$

for some distribution of points x_j, $j=0,\cdots,N$, in $[-1,1]$, and corresponding discrete weights, $\tilde{\omega}_j$.

The discrete orthogonal polynomial least squares (DOP-LS) approximation of a smooth function $f(x)$ in $[-1,1]$ is [13]:

$$P_{M,N}f(x)=\sum_{k=0}^{M}a_{k,N}\phi_k^\omega(x), \tag{2.20}$$

where

$$a_{k,N}=\frac{1}{h_k}<f,\phi_k^\omega>, \tag{2.21}$$

and $M<N$. The decay rate of the coefficients (2.21) depends on the smoothness properties of the underlying function $f(x)$ and on the choice of the discrete orthogonal polynomials $\phi_k^\omega(x)$, [13, 29]. For symmetric $\omega(x)$, the discrete orthogonal polynomials $\phi_k^\omega(x)$, $k=0,\cdots M$, can be determined from Stieltjes recurrence relation, [13], as

$$\phi_{k+1}^\omega(x)=x\phi_k^\omega(x)-\frac{h_k}{h_{k-1}}\phi_{k-1}^\omega(x), \tag{2.22}$$

where $\phi_0^\omega(x) = 1$ and $\phi_1^\omega(x) = x$.[‡]

We point out that the three-term recurrence formula above is sensitive to round-off errors and reorthogonalization may be needed. Instead, in our code we subtract the orthogonal projections of $x\phi_k^\omega$ against all polynomials of lower degree in the basis using a modified Gram-Schmidt iteration to avoid numerical instability, [27].

Since we are performing a least squares approximation, rather than interpolation, we are not limited to using a clustered distribution of points to guarantee convergence near the boundaries. Instead we choose to use equally spaced grid points, $x_j = -1 + j\Delta x$, $j = 0, \cdots, N$, with $\Delta x = \frac{2}{N}$, as this will help to relax the time step restriction when solving partial differential equations. The approximation can be optimized for any point distribution, however.

We pause here to note that $\phi_k^\omega(x) \rightarrow \psi_k^\omega(x)$, the continuous orthogonal polynomials defined in (2.2), for all k provided that the discrete inner product (2.19) converges to the continuous inner product (2.4) as $N \rightarrow \infty$, [13]. However, since N is finite and the point distribution is not Gaussian, this convergence is not exponential. As the convergence of the least squares approximation to a smooth function does not inherently depend on the type of the orthogonality of the expansion basis, we do not attempt to approximate $\psi_k^\omega(x)$ from the non-classical weight function $\omega(x)$. An accurate approximation of the least squares coefficients (2.21) would require far more grid points, and in fact the DOP-LS approximation would be less accurate. Thus the construction of (2.20) is both simplified and more efficient.

The problem can now be stated as follows: Given $f(x)$ at uniform grid points, x_j, $j = 0, \cdots, N$, we seek weight functions $\omega(x)$, and corresponding discrete weights $\tilde{\omega}_j$, so that the coefficients (2.21) decay exponentially. Subsequently, the DOP-LS approximation (2.20) will converge exponentially to smooth $f(x)$ in $[-1,1]$, assuming a slower growth rate of the expansion polynomials.

To obtain exponential decay of the least squares coefficients (2.21), we recall that if $g(x)$ is smooth and periodic with smooth and periodic derivatives, then the trapezoidal rule

$$\Delta x \sum_{j=1}^{N-1} g(x_j) + \frac{\Delta x}{2}(g(x_0) + g(x_N)) \tag{2.23}$$

converges exponentially to $\int_{-1}^{1} g(x)dx$, [3]. Hence for

$$g(x) = \frac{f(x)\phi_k^\omega(x)\omega(x)}{h_k}, \tag{2.24}$$

with $\omega(x)$ satisfying (2.11) for large $q(N)$, it follows that the DOP-LS coefficients $a_{k,N}$ in (2.21) decay exponentially. Here $\tilde{\omega}_j$ is defined by (2.14) for the weighted inner product calculation (2.19) of $a_{k,N}$.

[‡]For ease of presentation we only consider $\omega(x)$ to be symmetric. There is also a recursion formula corresponding to non-symmetric weight functions, [13].
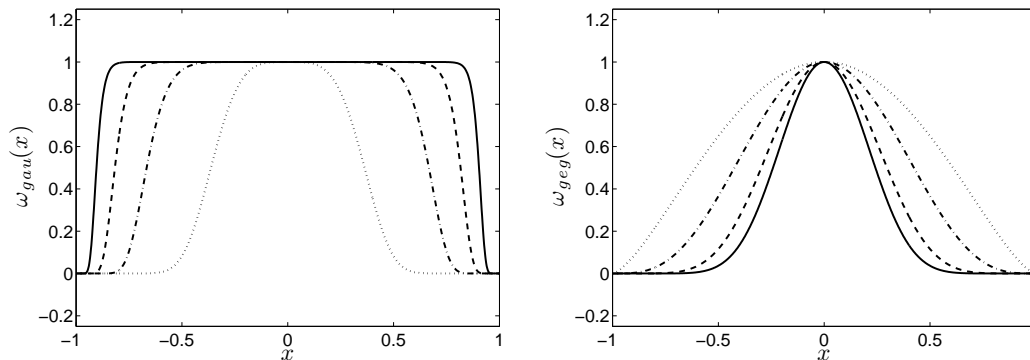
Figure 1: (left) Supper Gaussian weights $\omega_{gau}(x)$ for $\lambda=2$ (dotted), 5 (dash-dotted), 10 (dashed), and 20 (solid). (right) Gegenbauer weights $\omega_{geg}(x)$ for $q(N)=2$ (dotted), 4 (dash-dotted), 8 (dashed), and 12 (solid).

2.4 Super Gaussian weight functions

We now turn our attention to constructing weight functions that satisfy (2.11). As first described in [17] in the context of Fourier (pseudo-)spectral reprojection, and explored further in [15] for the DOP-LS approximation, the super Gaussian weight function defined as

$$\omega_{gau}(x):=e^{-\alpha x^{2\lambda}}, \qquad x\in[-1,1], \tag{2.25}$$

numerically satisfies (2.11) when $\alpha=-\ln\epsilon_M$ with ϵ_M representing machine accuracy.[§] Fig. 1 (left) displays the super Gaussian weight functions for several choice of λ. Note that as λ increases, $\omega_{gau}(x)=1$ over more of the interval $[-1,1]$. Since $\omega_{gau}(x)$ is smoothly connected to zero at ±1 up to machine precision, (2.23) implies that the discrete orthogonal polynomial coefficients, (2.21), decay exponentially.

Until now we have only made use of the weight function property (2.11), which holds for both the super Gaussian weight functions and the Gegenbauer weight functions for large $q(N)$. The other desirable property of the super Gaussian weight functions is that $\omega_{gau}(x)=1$ in most of the interval $[-1,1]$. As stated previously, this is not true for the Gegenbauer polynomial weight functions. As is evident in Fig. 1 (right), the interval for which $\omega_{geg}(x)=1$ shrinks as its number of continuous derivatives, $q(N)$, increase. Such behavior was recognized as a hindrance for the spectral reprojection method when Gegenbauer polynomials were used as the reprojection basis. In particular, it is responsible for the round-off error caused by the large growth of the Gegenbauer polynomials and also the effects of the generalized Runge phenomenon, [2, 16, 17].

In [17], the notion of a *robust* Gibbs complement was introduced for the spectral reprojection method to reduce these errors. Specifically, the weight function of a reprojection polynomial basis must satisfy

    1. $\omega(x)$ smoothly decays to zero at ±1.

[§]In [15, 17], (2.25) were referred to as Freud weights.

2. As the number of grid points N increases, $\omega(x) \to 1$ except at the points $x = \pm 1$.

The first requirement is met by any weight function satisfying (2.11). The second is met by the super Gaussian weight functions (2.25) for large λ. In fact, as λ increases, the growth of the corresponding polynomials decreases, and the effects of the generalized Runge phenomenon and round-off error of the spectral reprojection approximation are diminished.

The relationship between the weights in the DOP-LS method and those for a robust spectral reprojection is intentional. Due to the interpolatory properties of Fourier collocation, one can view the pseudo-spectral Fourier reprojection, (2.12), as a least squares orthogonal polynomial approximation method, [15]. This observation suggests that the same weights that reduce the Runge phenomenon, or equivalently increase the radius of convergence in the approximation, could be used to construct the DOP-LS approximation, (2.20). Hence we insist that $\omega(x) = 1$ in most of $[-1, 1]$. In addition to being less susceptible to round-off error and the Runge phenomenon, we see that much of information from the underlying function is used in the approximation. Specifically, if we define

$$\beta = \beta(M,N) = \frac{M}{N} = \frac{\text{\# of expansion terms}}{\text{\# of grid points}} \tag{2.26}$$

as the aspect ratio of (2.20), then a nearly constant β implies that the number of grid points N does not need to be very large to retain the characteristic features of the underlying function. Clearly $\beta < 1$ since $M \approx N$ returns an approximation resembling the poorly performing Lagrange interpolation. The second requirement is also essential when using the DOP-LS method for solving partial differential equations. Otherwise the numerical solution would only come from the interior of the domain, in regions far away from the boundary. Some additional considerations are necessary at the boundaries, since the weight function is zero there. This will be discussed further in Section 3.

Before demonstrating the effectiveness of the DOP-LS method, we make the following remarks:

1. The DOP-LS approximation can be calculated directly from the discrete data as

$$P_{M,N}f(x) = \sum_{j=0}^{N} f(x_j) g_j^\omega(x), \tag{2.27}$$

   where

$$g_j^\omega(x) = \tilde{\omega}_j \sum_{k=0}^{M} \frac{\phi_k^\omega(x_j)\phi_k^\omega(x)}{h_k}, \tag{2.28}$$

   can be described as pseudo-cardinal functions with $\tilde{\omega}_j$ defined in (2.14) and $\phi_k^\omega(x)$ is determined from (2.22).

2. The first derivatives of the discrete orthogonal polynomials, $\frac{d\hat{\phi}_l^\omega}{dx}(x)$, are easily constructed from (2.22). The DOP-LS approximation for $f'(x)$ can then be computed

as

$$\frac{d}{dx}P_{M,N}f(x) = \sum_{k=0}^{M} a_{k,N}\frac{d\phi_k^\omega}{dx}(x),$$

or equivalently

$$\frac{d}{dx}P_{M,N}f(x) = \sum_{j=0}^{N} f(x_j)\frac{dg_j^\omega}{dx}(x), \tag{2.29}$$

using the pseudo-cardinal functions in (2.28). Applying (2.29) may be more useful in implementing numerical methods for partial differential equations.
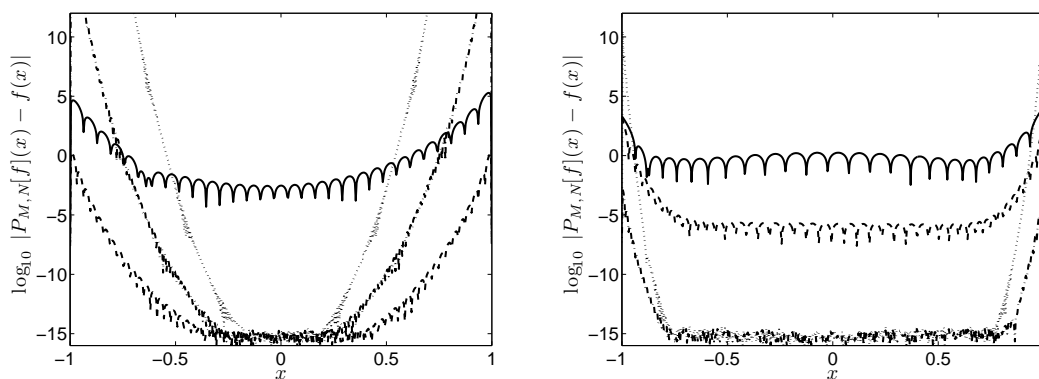

Figure 2: Pointwise errors in logarithmic scale for Example 2.1. (left) The DOP-LS approximation (2.20) used as an interpolation. (right) The DOP-LS approximation when $\beta = 0.7$. Here $N = 32$ (solid), 64 (dashed), 128 (dash-dotted), and 256 (dotted).

2.5 The DOP-LS approximation

The following examples illustrates the DOP-LS approximation (2.20) with respect to the super Gaussian weight function (2.25) for a smooth function in $[-1,1]$. In each case the grid points are uniformly distributed with $\Delta x = \frac{2}{N}$.

Example 2.1.

$$f(x) = \cos(10.4\pi x) + \sin(10.4\pi x), \quad x \in [-1,1]. \tag{2.30}$$

Fig. 2 displays the maximum error over the domain $[-1,1]$ for Example 2.1 using the DOP-LS method (2.20) for the aspect ratio $\beta = 1$, (interpolation, $M = N$) and $\beta = .7$, with $\lambda = .2N$ in (2.25). As expected, choosing $M = N$ produces the Runge phenomenon. Choosing $M = \text{round}(.7N)$, however, allows high order convergence throughout $[-1,1]$ and alleviates the Runge phenomenon. These results concur with those in [15].

The right plot of Fig. 2 illustrates that the error is actually machine precision in the majority of the domain, $[-\delta,\delta] \in [-1,1]$, when $N \geq 128$. This information is critical in defining our (overlapping) domains when solving partial differential equations with the DOP-LS method. On the one hand, δ should be as close to one as possible. In this case, the accurate approximation coming from the uniform point distribution in $[-1,1]$ will cover the majority of the domain, and will in turn relax the time stepping restrictions. On the other hand, the aspect ratio β should be nearly constant so that the method does not require many more original grid points N to resolve the function. These ideas are discussed further in Section 3.
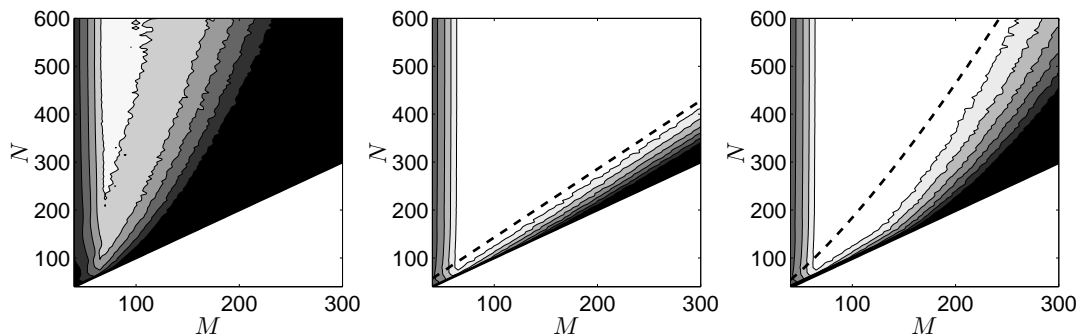

Figure 3: Contour plots of the L_∞ error in $[-\delta,\delta]$ as a function of N and M (with $M \leq N$) for Example 2.1. Contour levels are (white) $10^{-13}, 10^{-10}, 10^{-7}, 10^{-4}, 10^{-1}, 10^2$ (black). (left) $\delta = 1$. (center) $\delta = .75$ (right) $\delta = \max(.75, 1 - 20\Delta x)$. The dashed lines are the graphs of $M = .7N$, and $M = 2N^{3/4}$.
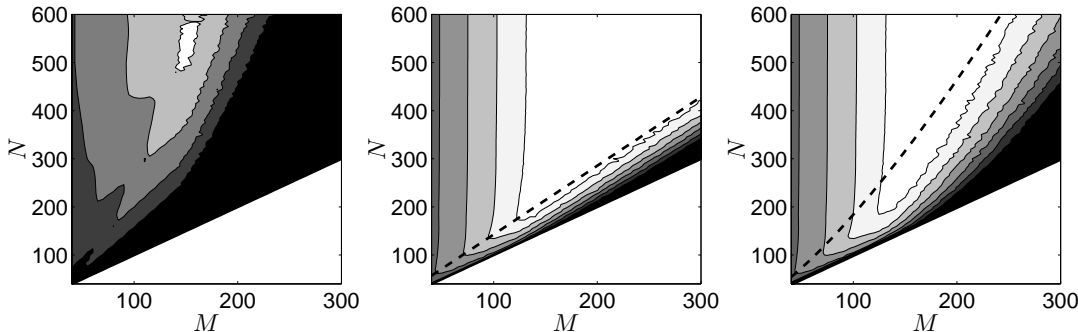

Figure 4: Contour plots of the L_∞ error in $[-\delta,\delta]$ as a function of N and M (with $M \leq N$) in Example 2.2. Contour levels are (white) $10^{-13}, 10^{-10}, 10^{-7}, 10^{-4}, 10^{-1}, 10^2$ (black). (left) $\delta = 1$. (center) $\delta = .75$ (right) $\delta = \max(.75, 1 - 20\Delta x)$. The dashed lines are the graphs of $M = .7N$, and $M = 2N^{3/4}$.

Fig. 3 demonstrates how a suitable aspect ratio (2.26) is chosen for $\delta = 1$, $\delta = 0.75$, and $\delta = \max(.75, 1 - 20\Delta x)$ when the DOP-LS method applied to Example 2.1. If we insist on having an accurate approximation in the entire interval, then a linear relationship between M and N is impossible. The largest aspect ratio requires $M \leq C\sqrt{N}$. This result is in agreement with the theoretical bounds in [26] and the numerical experiments in [1] for constant weights. The center plot demonstrates that for $M < 0.7N$, it is possible to obtain
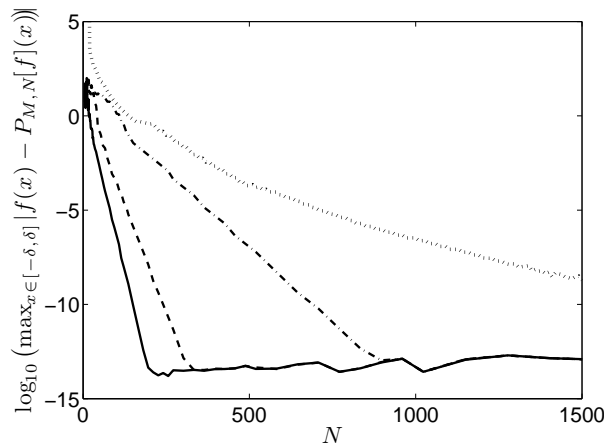
Figure 5: Log_{10} of the L_∞ error in $[-\delta,\delta]$ for Example 2.2: $\delta=0.75$ and $M=\mathrm{round}(0.65N)$ (solid), $\delta=0.90$ and $M=\mathrm{round}(0.42N)$ (dashed), $\delta=0.99$ and $M=\mathrm{round}(0.15N)$ (dash-dotted), and $\delta=1$ and $M=\mathrm{round}(4\sqrt{N})$ (dotted).

machine precision in $[-.75,.75]$. The right plot illustrates that exponential convergence is possible as $\delta \to 1$ with $M=\mathcal{O}(N^{3/4}))$ instead of $\mathcal{O}(\sqrt{N})$ for practical choices of N. Of course the minimum M is determined by the resolution requirements of the particular example. In this case, $M>50$. Note that information from the original data, $f(x_j)$, $j=0,\cdots,N$, in entire interval $[-1,1]$ is still used to obtain the approximation in any sub-interval $[-\delta,\delta]$.

In the following example, we test the convergence of the DOP-LS approximation for a function that is analytic in $[-1,1]$ but has poles in the complex plane at $z=\pm 0.25i$. Polynomial interpolation on equidistant points for this class of functions is known to diverge exponentially fast (Runge phenomenon). We used this example to illustrate how discrete least squares can be used to avoid Runge oscillations.

Example 2.2.

$$f(x)=\frac{1}{x^2+\frac{1}{16}}, \qquad x\in[-1,1]. \tag{2.31}$$

Fig. 4 displays the contours of the maximum errors for the DOP-LS method for M vs. N for Example 2.2 using the super Gaussian weights in both $[-1,1]$ and $[-.75,.75]$. We also show the maximum error in the interval $[-\delta,\delta]$, for increasing δ for various choices of M and $N=128$ in Fig. 5.

Both examples demonstrate that high order accuracy is obtainable in any interval if M is chosen to be proportional to $\sqrt{N}$. For constant aspect ratio β in (2.26), however, the approximation error is still very small in $[-\delta,\delta]$ when $\delta \leq .75$, and we can still obtain machine precision as $\delta \to 1$ without decreasing the aspect ratio to $\frac{c\sqrt{N}}{N}$. We use this result to develop a highly accurate hybrid (overlapping) multi-domain method for solving partial

differential equations. The majority of the computation is performed on equally spaced points, and as a consequence, the usually very restrictive time step (e.g., for traditional orthogonal polynomial spectral methods) can be somewhat relaxed. This is the topic of discussion in Section 3.
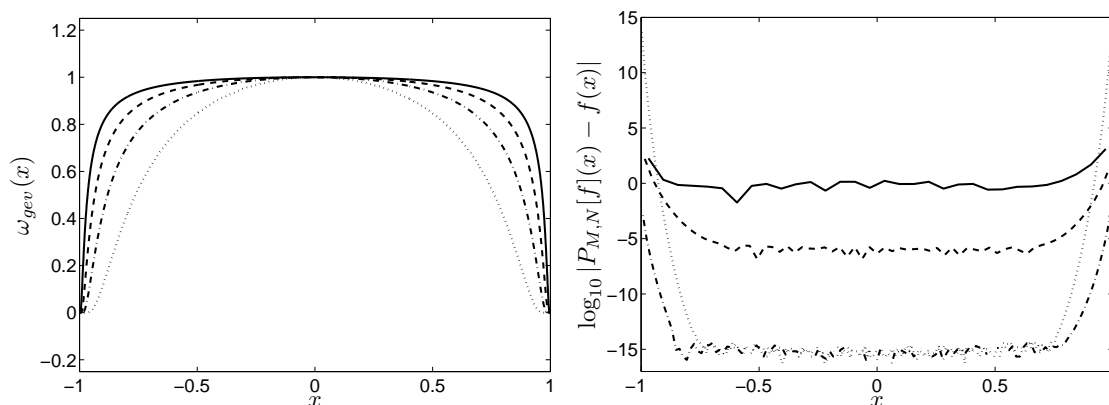

Figure 6: (left) Gevrey weights $\omega_{gev}(x)$ for $\lambda=2$ (dotted), 5 (dash-dotted), 10 (dashed), and 20 (solid). (right) Pointwise error for Example 2.1 with Gevrey weights, $\beta=0.7$, and $\lambda=\mathrm{round}(0.05N)$. Here $N=32$ (solid), 64 (dashed), 128 (dash-dotted), 256 (dotted).

2.6   Other qualifying weight functions

It is possible to construct other weight functions that satisfy (2.11) so that $\omega(x) \to 1$ in $(-1,1)$. For example, in [32] the authors suggested a modified Gegenbauer weight for spectral reprojection,

$$\omega(x) = (1-x^2)^{q(N)-\frac{1}{2}}e^{-\alpha x^2}.$$

Here α is chosen so that $\omega(\pm 1) \approx \mathcal{O}(\epsilon_M)$, where ϵ_M is machine precision. This weight function can be made to satisfy both requirements for the spectral reprojection and DOP-LS method by modifying it as

$$\omega(x) = (1-x^2)^{q(N)-\frac{1}{2}}e^{-\alpha x^{2\lambda}}.$$

Below we consider the Gevrey weight function, which is defined as

$$\omega_{gev}(x) := \left\{ \begin{array}{ll} \exp\left(\frac{x^2}{\lambda(x^2-1)}\right), & 0 < |x| < 1, \\ 0, & |x| \geq 1. \end{array} \right. \tag{2.32}$$

The Gevrey weight function has been studied in the context of spectral mollifiers, [33,34], and has also been proposed as an alternative for constructing the spectral reprojection basis, [17].[¶]   The Gevrey weight function is more easily characterized than the super Gaussian weight function due to its compact support on $[-1,1]$.

[¶]Technically the corresponding Gevrey polynomials produce only root exponential accuracy.

Fig. 6 demonstrates that the DOP-LS approximation method using (2.32) also yields fast convergence for Example 2.1. In fact, our experiments indicate that by choosing appropriate parameters, Gevrey and super Gaussian weights produce comparable approximations.

3   Solving partial differential equations using the DOP-LS method

Although it is possible to approximate a smooth function in the entire interval $[-1,1]$ using the DOP-LS method (2.20), Examples 2.1 and 2.2 both indicate that limiting the approximation to the interval $[-\delta,\delta]$, $\delta<1$, significantly improves the convergence rate and maintains a constant aspect ratio, (2.26). Hence the resolution requirements for the DOP-LS method are similar to those of other global expansion methods and therefore should not significantly increase the cost of the approximation. It is therefore feasible to use the DOP-LS method to develop a numerical algorithm for solving partial differential equations with smooth solutions. The idea is to use a hybrid (overlapping) multi-domain technique. That is, we use the DOP-LS method to approximate the solution on $[-\delta,\delta]$ from $N+1$ equally spaced points in $[-1,1]$. Then, we replace the "bad" DOP-LS solution in both boundary regions $[-1,-\delta]$ and $[\delta,1]$ with the standard Chebyshev interpolation on $N_{cheb}+1$ Gauss Lobatto points (in each region). Finally, the solution is patched across the internal boundaries $x=\pm\delta$. As $\delta=\delta(N)\to1$, the number of Chebyshev points required in each boundary region decreases. This technique lends itself to solving a (linear advection) PDE because the maximum allowable time step for an explicit method is proportional to $(1-\delta)N_{cheb}^{-2}$. Therefore, if $N_{cheb}\ll N$, the original number of points in $[-1,1]$, then it is possible to build a highly accurate method that is stable for a less restrictive time step.

Fig. 7 graphically illustrates the hybrid (overlapping) multi-domain idea. The DOP-LS method uses grid point information in $[-1,1]$ to approximate the solution in $[-\delta,\delta]$. As displayed in Fig. 7 (upper-right), the Runge phenomenon ruins the approximation in the boundary regions $[-1,-\delta]$ and $[\delta,1]$. Hence we throw away the DOP-LS solution in those regions and instead use Chebyshev interpolation there with $N_{cheb}=(1-\delta)N/2$ Gauss Lobatto points. Fig. 7 (lower-right) shows the final "patched" solution.

To solve a PDE, we first differentiate the solution at any given time step on the three overlapping sub-domains, employing the DOP-LS method on $[-1,1]$ and the Chebyshev method on $[-1,-\delta]$ and $[\delta,1]$. We then use an explicit time marching scheme (e.g., fourth order Runge-Kutta) to advance the solution on each (overlapped) sub-domain. Next, the Chebyshev solutions on $[-1,-\delta]$ and $[\delta,1]$ are projected back onto the original grid points. Finally, the solution is patched across the interior boundaries to ensure continuity. We note the similarity to more traditional multi-domain methods. Here, however, the approximation in the interior is produced from function data in all of $[-1,1]$, and not just from information in the interior domain $[-\delta,\delta]$, since we need all the information from $[-1,1]$ to achieve the spectral accuracy in $[-\delta,\delta]$ as $M\to N$.
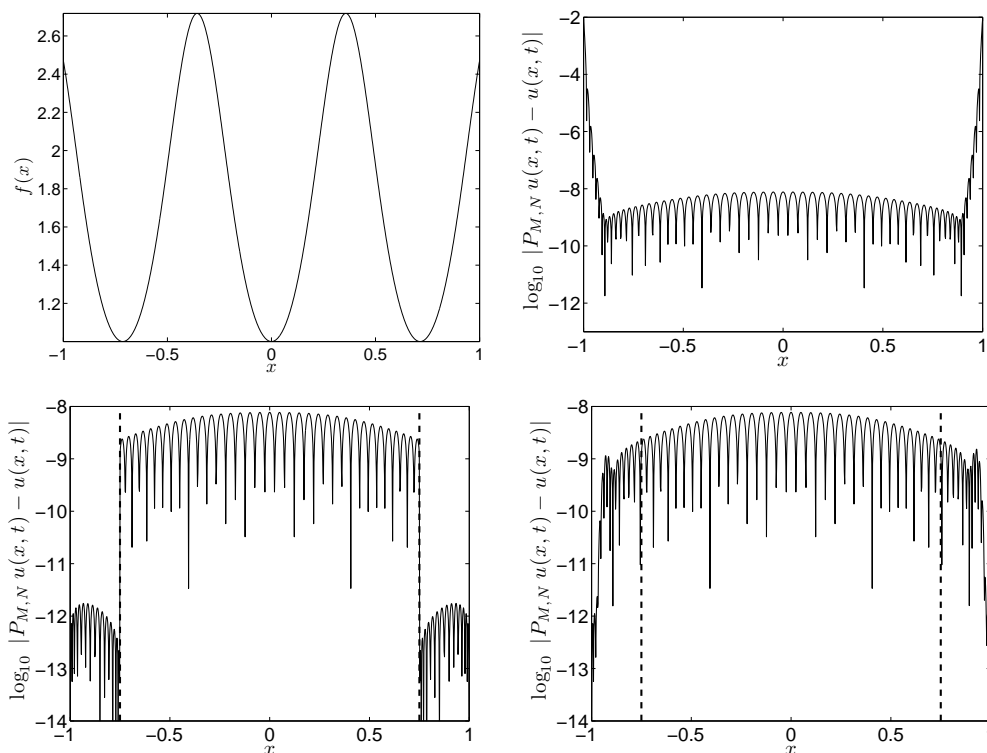
Figure 7: Hybrid approximation of $f(x) = \exp\left(\sin(1.4\pi x)^2\right)$. (upper-left) Graph of f in $[-1,1]$. (upper-right) Log of the error in the DOP-LS approximation with $N=128$ and $M=\text{round}\left(\min(0.5N, \frac{3}{2}N^{\frac{3}{4}}) = 57$. (lower-left) Error after the Chebyshev correction in $[-1,-.75]$ and $[.75,1]$ with $N_{cheb} = N_\delta = N/8 = 16$. (lower-right) Error after the smooth patching described in Algorithm 3.1.

3.1   The hybrid DOP-LS algorithm

Let us consider the one dimensional linear transport equation.

Example 3.1.

$$u_t + u_x = 0, \qquad x \in (-1,1), \tag{3.1}$$

with boundary conditions $u(-1,t) = B(t)$ and initial conditions $u(x,0) = f(x)$.

Assume that $B(t)$ is such that the solution $u(x,t)$ is smooth. The algorithm below describes how the hybrid overlapping multi-domain (hybrid DOP-LS) method works for Example 3.1.

Algorithm 3.1 (hybrid DOP-LS).

1. The domain $[-1,1]$ is divided into three overlapping sub-intervals, $[-1,1]$, $[-1,-\delta]$ and $[\delta,1]$.

2. We assume $u(x,0)$ can be calculated on any grid points. In $[-1,1]$, the grid points are $x_j = -1 + \frac{2j}{N}$, $j = 0, \cdots, N$. In $[-1, -\delta]$ and $[\delta, 1]$, we make the linear transformation onto the Chebyshev domain $\xi \in [-1,1]$

$$x = a\xi + b.$$

Here $a = (1-\delta)/2$, $b = -(1+\delta)/2$ in $[-1, -\delta]$, and $b = (1+\delta)/2$ in $[\delta, 1]$. We then determine $u(x(\xi), 0)$ on Chebyshev points in each boundary region, with $\xi_i = -\cos(\pi i / N_{cheb})$, $i = 0, \cdots, N_{cheb}$.

3. The DOP-LS derivative approximation is then constructed for u_x from (2.29).

4. Standard Chebyshev differentiation techniques is used to compute

$$u_x = u_\xi \frac{d\xi}{dx} = \frac{2}{1-\delta} u_\xi$$

in $[-1, -\delta]$ and $[\delta, 1]$ on the transformed variable $\xi \in [-1,1]$.

5. Example (3.1) is advanced in time in all of the three (overlapping) sub-domains using the fourth order Runge Kutta method. There are now three approximations at the each intermediate time step:

   (a) $u_{gauss}(x)$ on equally spaced points in $[-1,1]$,
   (b) $u_{cheb}(x(\xi))$ on Chebyshev points in $[-1, -\delta]$, and
   (c) $u_{cheb}(x(\xi))$ on Chebyshev points in $[\delta, 1]$.

6. Since the characteristics move left to right, we impose the boundary condition $u_{cheb}(-1, t) = B(t)$ on the left Chebyshev domain $[-1, -\delta]$. An inflow condition is also needed on the right Chebyshev domain $[\delta, 1]$ at $x = \delta$. Since $u_{gauss}(x)$ is accurate in the domain $[-\delta, \delta]$, we use $u_{cheb}(\delta) = u_{gauss}(\delta)$.

7. The calculation of $u_{gauss}(x)$ outside $[-\delta, \delta]$ is not very good, so it is replaced by projecting the Chebyshev approximation u_{cheb} back onto the equally spaced points that fall in the interval $[-1, -\delta]$, x_j, $j = 0, \cdots, N_\delta$, where $N_\delta = int(\frac{N(1-\delta)}{2})$:

$$u_{cheb}(x_j) = \sum_{i=0}^{N_{cheb}} u_{cheb}(x(\xi_i)) h_i(x_j).$$

Here $h_i(x_j)$ is the usual Chebyshev cardinal function given by

$$h_i(x_j) = \frac{2}{N_{cheb} c_i} \sum_{l=0}^{N_{cheb}} \frac{T_l(\xi_i) T_l(x_j)}{c_l} = \frac{1}{N_{cheb}^2 c_i} \frac{(1 - x_j^2) T'_{N_{cheb}}(x_j)}{(x_j - \xi_i) T_{N_{cheb}}(\xi_i)},$$

where $T_l(\cdot)$ are the Chebyshev polynomials and

$$c_i = \begin{cases} 2, & \text{if } i = 0 \text{ or } i = N_{cheb}, \\ 1, & \text{otherwise.} \end{cases}$$

The same projection is done in $[\delta, 1]$ for x_j, $j = N - N_\delta, \cdots, N$.

8. To create a smooth interface at $x = \pm\delta$, the approximations are "patched" across the left and right intervals. The transition should be as quick and smooth as possible, so that the Runge effects from the boundary region of $u_{gauss}(x)$ do not interfere with the accurate solution $u_{cheb}(x)$. Hence we define

$$p(x) = e^{-\alpha\left(\frac{-\delta-x}{1-\delta}\right)^{2q}}.$$

Here α is chosen so that $p(-1) \approx \mathcal{O}(\epsilon_M)$, where ϵ_M is machine precision. We use $q = 4$ to ensure the quick transition of the patching function.[‖] The updated solution in $[-1, -\delta]$ is then

$$u(x) = p(x)u_{gauss}(x) + (1 - p(x))u_{cheb}(x).$$

A similar patching function $p(x)$ is constructed for $[\delta, 1]$. The approximation in the interval $[-\delta, \delta]$ is unchanged.

9. We can now start the process again at the next time level with the approximations $u(x)$ on uniform points in $[-1, 1]$, and $u_{cheb}(x(\xi))$ on Chebyshev Gauss Lobatto points in $[-1, -\delta]$ and $[\delta, 1]$.

Remark 3.1.

1. We chose symmetric boundary regions for ease of implementation. Depending on the underlying solution, it may be appropriate to choose intervals of different length.

2. The super Gaussian polynomials, Chebyshev polynomials, derivative matrices and Chebyshev cardinal functions are only computed once and subsequently stored.

3. The endpoints of the Chebyshev intervals must coincide with the grid point distribution of the DOP-LS approximation to avoid unnecessary discontinuities when the Chebyshev solution is projected onto the equally spaced points. Thus δ should be adjusted accordingly.

4. We can use $\Delta t = (1 - \delta)N_{cheb}^{-2}$ in accordance to Runge Kutta stability criteria for Chebyshev methods. The amount of increased efficiency therefore depends upon the aspect ratio value β in (2.26) and the boundary region length $1 - \delta(N)$.[**]

The main advantages in using the DOP-LS approximation in the hybrid overlapping domain approach appear to be that 1) any grid point distribution can be used for the least squares approximation and 2) the corresponding stability requirement on the time step is

---

[‖]This patching function also ensures that the solution in $[-1, -\delta]$ and $[\delta, 1]$ is still the solution from the original underlying equation. Since the Chebyshev solution is the only accurate solution of the PDE in the boundary region, any kind of averaging from the solution that comes from the neighboring domain might alter the PDE so that it no longer represents the physics of the solution.

[**]While N_δ is determined by δ, we do not necessarily need to choose $N_{cheb} = N_\delta$. In fact, selecting a smaller N_{cheb} will accelerate time advancement, although possibly at the cost of overall accuracy.
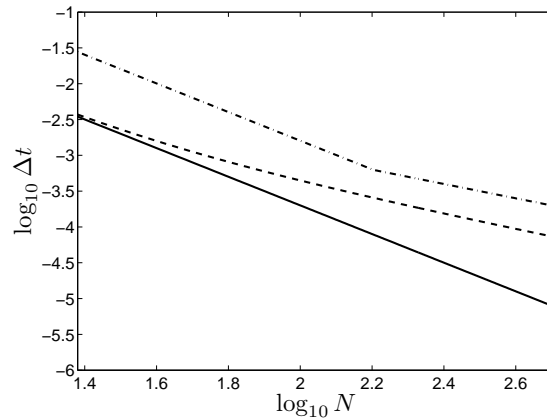
Figure 8: Loglog plot of the theoretical maximum Δt when $\alpha = 1$ for the hybrid DOP-LS (dash-dotted), Chebyshev (solid), and mapped Chebyshev (dashed).

less restrictive than for typical orthogonal polynomial spectral methods. The first point is left for future investigations. We examine the stability requirements below.

The time step for Algorithm 3.1 for the one dimensional transport problem is

$$\Delta t_{hybrid} = \frac{\alpha(1-\delta)}{N_{cheb}^2}, \qquad (3.2)$$

where α depends upon the numerical time integration scheme and the wave speed of the equation. If $\delta(N) = \max(.75, 1 - 20\Delta x)$, then

$$N_{cheb} = N_\delta = \min\left(\frac{1-\delta}{2}N, 20\right) = \min\left(\frac{N}{8}, 20\right). \qquad (3.3)$$

Hence

$$\Delta t_{hybrid} = \max\left(\frac{16\alpha}{N^2}, \frac{\alpha}{10N}\right).$$

Thus the hybrid overlapping multi-domain scheme may be significantly more efficient than the standard Chebyshev and mapped Chebyshev methods [24, 25, 28], particularly if large N is needed to resolve the solution and if the aspect ratio (2.26) is close to being constant.

Fig. 8 shows how the theoretical lower bound on Δt changes for the Chebyshev, mapped Chebyshev, and DOP-LS methods for several values of N. For the mapped Chebyshev method, we used

$$\Delta t_{mapped} = \frac{\zeta}{\arcsin(\zeta)\sqrt{1-\zeta^2}}\Delta t_{Cheb}, \qquad \zeta = \left(\cosh\left(\frac{36}{N}\right)\right)^{-1},$$

as described in [25]. Notice that the hybrid method allows significantly larger time-steps than the other two methods, even for small values of N. Of course there are more operations per time step for the DOP-LS method, due to its hybrid nature. Further investigation is needed to determine the suitability of the technique for various applications.
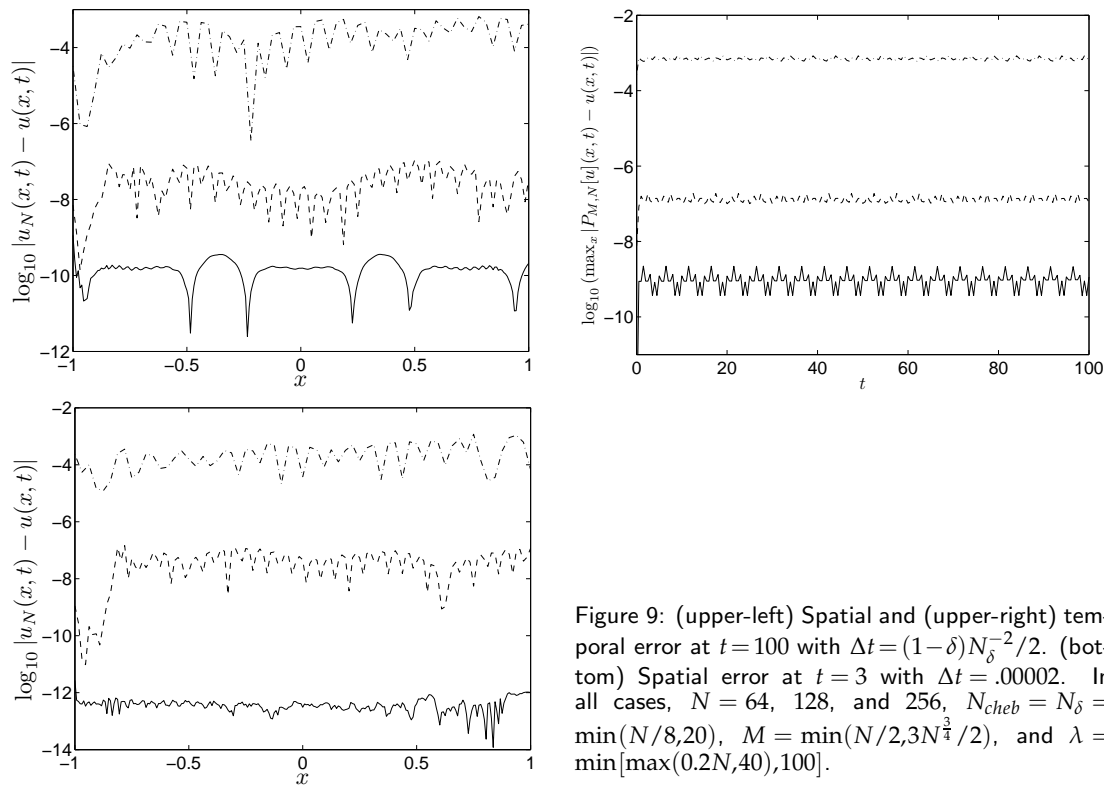
Figure 9: (upper-left) Spatial and (upper-right) temporal error at $t=100$ with $\Delta t=(1-\delta)N_\delta^{-2}/2$. (bottom) Spatial error at $t=3$ with $\Delta t=.00002$. In all cases, $N=64$, 128, and 256, $N_{cheb}=N_\delta=\min(N/8,20)$, $M=\min(N/2,3N^{\frac{3}{4}}/2)$, and $\lambda=\min[\max(0.2N,40),100]$.

4   Numerical results

We now validate our numerical method for the transport problem in Example 3.1 using the following initial and boundary conditions:

Example 4.1. Consider Eq. (3.1) with

$$u(x,0)=\exp(\sin(1.4\pi x)^2),$$
$$u(-1,t)=\exp(\sin(1.4\pi(1+t))^2).$$

We apply Algorithm 3.1 with $\delta=\max(.75,1-20\Delta x)$, $\lambda=\min(\max(.2N,40),100)$, and $M=\min(\frac{N}{2},\frac{3}{2}N^{\frac{3}{4}})$, which is a conservative choice based on the results in Fig. 3. Note that information generated through the boundary condition at $x=-1$ leaves the domain after time $t=2$. Hence it is reasonable to assume that with a Dirichlet boundary condition, the numerical solution would show instability before that time. The numerical results are shown in Fig. 9. These approximations were obtained using 32, 64, 128, and 256 points. The top graphs show the errors for $t=15$ using $\Delta t=(1-\delta)N_\delta^{-2}/2$. The error shown from $t=0$ to $t=15$ indicates that the solution is stable in time. The graph on the bottom shows how the spatial error decays at $t=1$ when $\Delta t=0.00002$ is used for all values of N.
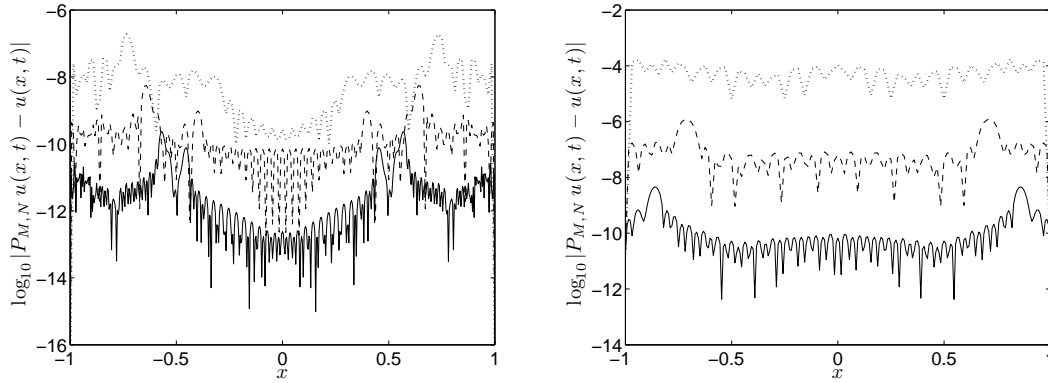
Figure 10: Spatial error in the numerical solution of Example 4.2 at (left) $t=0.5$ with $\Delta t=.00001$ and (right) $t=100$ with $\Delta t=(1-\delta)N_\delta^{-2}$. Here we used $N=64,128$, and 256.
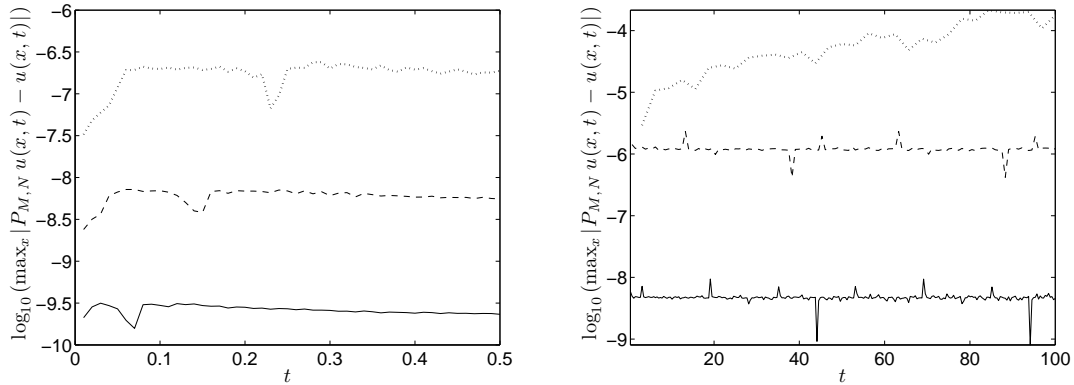

Figure 11: Temporal error in the numerical solution of Example 4.2 at (left) $t=0.5$ with $\Delta t=.00001$ and (right) $t=100$ with $\Delta t=(1-\delta)N_\delta^{-2}$. Here we used $N=64,128$, and 256.

Example 4.2. As a second example, consider the one dimensional acoustic problem

$$u_t=v_x, \qquad v_t=u_x, \qquad x\in(-1,1), \tag{4.1}$$

with initial conditions $u(x,0)=\exp(-24x^2)$ and $v(x,0)=0$, and boundary conditions $u(-1,t)=u(1,t)=0$.

We apply Algorithm 3.1, modified for Example 4.2, with the same parameters as before. Following general multi-domain spectral methods stability requirements, characteristic decomposition is used to impose internal boundary conditions, [4]. Figs. 10 and 11 demonstrate the fast convergence of the hybrid method over long time periods. We note that no additional attempts were made to optimize the parameters to produce faster convergence or to ensure stability. It is evident from Fig. 11 (right) that long term instability occurs when $N=64$ for these parameters.

5 Conclusion

The DOP-LS approximation removes the Runge phenomenon and provides a highly accurate least squares approximation of smooth functions on $[-1,1]$. Furthermore, for a constant aspect ratio (2.26), the method yields machine precision accuracy in a large sub-interval, although the approximation in the boundary regions is poor. By employing Chebyshev interpolation to eliminate the Runge effects in the boundary region, we have developed the hybrid DOP-LS method for solving partial differential equations with smooth solutions. This is accomplished by using three overlapping domains. The DOP-LS solution in the majority of the domain at each time step comes from equidistant grid points in $[-1,1]$. The solution in the two smaller boundary regions are acquired by standard Chebyshev collocation.

For aspect ratio $\beta = \frac{M}{N} > \frac{\sqrt{N}}{N}$, the hybrid DOP-LS method might be more efficient than the (mapped) Chebyshev method. That is, if the number of Chebyshev points used in each boundary region can be made sufficiently small, then the hybrid DOP-LS method time step will be more like $\mathcal{O}(\frac{1}{N})$, rather than the usual $\mathcal{O}(\frac{1}{N^2})$. Further comparisons with the Chebyshev method will reveal under what conditions and for which types of PDEs the hybrid DOP-LS method may provide faster computation.

Finally, we note that the DOP-LS method can use any grid point distribution, not just equally spaced. This should prove useful in applications where the nodal distribution is dictated by other factors, such as when resolution requirements might vary throughout the numerical domain. This will be explored in future work.

Acknowledgments

References

[1] J. P. Boyd and F. Xu, Divergence (Runge phenomenon) for least-sqaures polynomial approximation on an equispaced grid and Mock-Chebyshev subset interpolation, J. Comput. Appl. Math., 2007, submitted.
[2] J. P. Boyd, Trouble with Gegenbauer reconstruction for defeating Gibbs' phenomenon: Runge phenomenon in the diagonal limit of Gegenbauer polynomial approximations, J. Comput. Phys., 204(1) (2005), 253-264.
[3] J. P. Boyd, Chebyshev and Fourier Spectral Methods, 2nd ed., Dover Publications, Mineola, New York, 2001.
[4] C. Canuto, M. Y. Hussaini, A. Quarteroni and T. A. Zang, Spectral Methods in Fluid Dynamics, Springer-Verlag, Berlin, 1988.
[5] H. Chen and B. D. Shizgal, The quadrature discretization method (QDM) in the solution of the Schrödinger equation, J. Math. Chem., 24 (1998), 321-343.

 [6] H. Chen and B. D. Shizgal, A spectral solution of the Sturm-Liouville equation: Comparison of classical and nonclassical basis sets, J. Comput. Appl. Math., 136 (2001), 17-35.
 [7] P. Davis, Interpolation and Approximation, Blaisdell Publishing Company, New York, 1963.
 [8] T. A. Driscoll and B. Fornberg, A Padé-based algorithm for overcoming the Gibbs phenomenon, Numer. Algorithms, 26 (2001), 77-92.
 [9] K. S. Eckhoff, Accurate reconstructions of functions of finite regularity from truncated series expansions, Math. Comput., 64 (1995), 671-690.
[10] B. Fornberg, A Practical Guide to Pseudospectral Methods, Cambridge University Press, Cambridge, 1996.
[11] G. Freud, Orthogonal Polynomials, Pergamon press, Oxford, 1971.
[12] R. D. M. Garcia, The application of nonclassical orthogonal polynomials in particle transport theory, Prog. Nucl. Energy, 35(3,4) (1999), 249-273.
[13] W. Gautschi, Orthogonal Polynomials: Computation and Approximation, Numerical Mathematics and Scientific Computation Series, Oxford University Press, 2004.
[14] J. Geer and N. S. Banerjee, Exponentially accurate approximations to piecewise smooth periodic functions, J. Sci. Comput., 12 (1997), 253-287.
[15] A. Gelb, Reconstruction of piecewise smooth function from non-uniform grid point data, J. Sci. Comput., 30(3) (2007), 409-440.
[16] A. Gelb, Parameter optimization and reduction of round off error for the Gegenbauer reconstruction method, J. Sci. Comput., 20(3) (2004), 433-459.
[17] A. Gelb and J. Tanner, Robust reprojection methods for the resolution of the Gibbs phenomenon, ACHA, 20(1) (2006), 3-25.
[18] D. Gottlieb and J. Hesthaven, Spectral methods for hyperbolic problems, J. Comput. Appl. Math., 128 (2001), 83-131.
[19] D. Gottlieb and S. Orszag, Numerical Analysis of Spectral Methods: Theory and Applications, SIAM, Philadelphia, 1977.
[20] D. Gottlieb and C.-W. Shu, On the Gibbs phenomenon and its Resolution, SIAM Rev., 30 (1997), 644-668.
[21] D. Gottlieb and C. W. Shu, A general theory for the resolution of the Gibbs phenomenon, Atti dei Convegni Lincei, 147 (1998), 39-48.
[22] D. Gottlieb, C. W. Shu, A. Solomonoff and H. Vandeven, On the Gibbs phenomenon I: Recovering exponential accuracy from the Fourier partial sum of a nonperiodic analytic function, J. Comput. Appl. Math., 43 (1992), 81-98.
[23] D. Gottlieb and E. Tadmor, Recovering pointwise values of discontinuous data within spectral accuracy, in: E. M. Murman and S. S. Abarbanel (Eds.), Progress and Supercomputing in Computational Fluid Dynamics, Proceedings of a 1984 U.S.-Israel Workshop, Progress in Scientific Computing, Vol. 6, Birkhauser, Boston, 1985, pp. 357-375.
[24] J. S. Hesthaven, P. G. Dinesen and J. P. Lynov, Spectral collocation time-domain modelling of diffractive optical elements, J. Comput. Phys., 155(2) (1999), 287-306.
[25] D. Kosloff and H. Tal-Ezer, A modified Chebyshev pseudospectral method with $\mathcal{O}(N^{-1})$ time restriction, J. Comput. Phys., 104(2) (1993), 457-469.
[26] A. B. J. Kuijlaars and E. A. Rakhmanov, Zero distributions for discrete orthogonal polynomials, J. Comput. Appl. Math., 99 (1998), 255-274.
[27] S. Leon, Linear Algebra with Applications, Prentice Hall, New Jersey, 2002.
[28] J. L. Mead and R. A. Renaut, Accuracy, resolution and stability properties of a modified Chebyshev method, SIAM J. Sci. Comput., 24(1) (2002), 143-160.
[29] A. F. Nikiforov, S. K. Suslov and V. B. Uvarov, Classical Orthogonal Polynomials of a Discrete

Variable, Springer-Verlag, 1991.

[30] G. Szego, Orthogonal Polynomials, American Mathematical Society, Providence, 1939.

[31] B. Shizgal, Spectral methods based on nonclassical basis functions: The advection-diffusion equations, Comput. Fluids, 31 (2002), 825-843.

[32] B. Shizgal and J.-H. Jung, Towards the resolution of the Gibbs phenomena, J. Comput. Appl. Math., 161 (2003), 41-65.

[33] E. Tadmor and J. Tanner, Adaptive mollifiers – high resolution recovery of piecewise smooth data from its spectral information, J. Foundations Comput. Math., 2 (2002), 155-189.

[34] J. Tanner, Optimal filter and mollifier for piecewise smooth spectral data, Math. Comput., 75 (2006), 767-790.